applied sciences

MDPI

Article

L-Lysine-Based Dendritic Coatings with Antimicrobial and Hydrophobic Properties for Preventive Conservation of Natural Stone

Mariana Barroso [1], Sérgio Martins [1], Luís Dias [1], Maria Margarida Calhaco [1], Mafalda Costa [1], Ana Teresa Caldeira [1,2], José Mirão [1,3] and Pedro Barrulas [1,2,*]

[1] HERCULES—Cultural Heritage Studies and Protection, IN2PAST—Associate Laboratory for Research and Innovation in Heritage, Arts, Sustainability and Territory, University of Évora, Palácio do Vimioso, Largo Marquês de Marialva 8, 7000-809 Évora, Portugal; marianacfbarroso@gmail.com (M.B.); smam@uevora.pt (S.M.); luisdias@uevora.pt (L.D.); mmcalhaco@gmail.com (M.M.C.); mcosta@uevora.pt (M.C.); atc@uevora.pt (A.T.C.); jmirao@uevora.pt (J.M.)

[2] Chemistry and Biochemistry Department, Sciences and Technology School, University of Évora, Colégio Luís António Verney, Rua Romão Ramalho, 59, 7000-671 Évora, Portugal

[3] Geosciences Department, Sciences and Technology School, University of Évora, Colégio Luís António Verney, Rua Romão Ramalho, 59, 7000-671 Évora, Portugal

* Correspondence: pbarrulas@uevora.pt

Abstract

Natural stone used in cultural heritage is highly susceptible to deterioration driven by environmental, chemical, and biological factors, with microbial biodeterioration and water playing a critical role in physicochemical and aesthetic degradation. Therefore, this study aimed to develop innovative organic coatings with antimicrobial and hydrophobic properties based on dendritic polymers derived from L-lysine functionalized with different fatty acids. Dendrons of generations G0 and G1 were synthesized via amidation and hydrolysis reactions, followed by structural characterization using NMR, FTIR and mass spectrometry, and their antimicrobial activity was evaluated against microorganisms associated with biodeterioration, alongside assessments of hydrophobic performance, aesthetic compatibility and durability on natural stone substrates. The results showed that antimicrobial activity and hydrophobic performance depended on the dendritic architecture, fatty acid chain length, and stone substrate. Most formulations also exhibited acceptable colorimetric compatibility after accelerated ageing. Overall, these findings highlight the potential of the developed coatings as a promising, sustainable, and effective strategy for protecting natural stone against the deleterious effects of water, contributing to the mitigation of biodeterioration and the conservation of cultural heritage assets.

Keywords: biodeterioration; dendritic coatings; heritage protection; hydrophobic coatings; sustainability

Check for updates

Academic Editor: Asterios Bakolas

Received: 19 August 2026
Revised: 19 October 2026
Accepted: 20 October 2026
Published: 23 October 2026

Copyright: © 2026 by the authors. Licensee MDPI, Basel, Switzerland. This article is an open access article distributed under the terms and conditions of the Creative Commons Attribution (CC BY) license.

1. Introduction

Natural stone has been highly used worldwide in archaeological, historical, and contemporary architecture due to its durability, aesthetic value, and cultural significance [1–10]. Consequently, the preservation of stone-built cultural heritage has become a major scientific and societal concern, particularly considering the progressive deterioration observed in monuments and historical structures exposed to environmental conditions over long

periods of time [1,2,4,11–15]. Stone degradation results from the combined action of anthropogenic and natural factors, including atmospheric pollution, thermal stress, weathering processes, water infiltration, salt crystallization, and biological colonization [1–3,5,11,14,16].

Among the different deterioration mechanisms affecting stone materials, biodeterioration is considered one of the most relevant processes compromising both the aesthetic and physicochemical integrity of cultural heritage substrates [6,13,15,17–20]. Biodeterioration is mainly associated with the colonization and metabolic activity of microorganisms such as bacteria, fungi, algae, and lichens, which develop biofilms on stone surfaces and induce discoloration, mineral dissolution, biocorrosion, and surface erosion [1,5,6,11,13,15,18–21]. In addition to aesthetic damage, microbial communities may penetrate fissures and pores, contributing to structural weakening and accelerating degradation phenomena [3,5,9,11,15,17–19,22,23].

The susceptibility of stone materials to microbial colonization is strongly influenced by their intrinsic physicochemical properties, particularly porosity, roughness, permeability, and mineralogical composition [1,2,4,10,13,19,23–26]. Highly porous substrates promote water retention and create favourable microenvironments for microbial growth and biofilm formation. In fact, water is recognized as one of the most critical external agents involved in stone deterioration, acting not only as a determining factor for microbial proliferation, but also as a transport medium for soluble salts and pollutants [1,4,11,12,27–29]. Therefore, water infiltration may promote chemical dissolution and trigger freeze–thaw cycles and salt crystallization within the stone pore network; the latter two processes generate internal mechanical stresses, thereby progressively compromising the material's durability [1,3,27,28].

To mitigate the effects of water-induced deterioration and microbial colonization, various protective strategies have been proposed for stone conservation, including mechanical, physical, biological, and chemical treatments [28,30–33]. Among these approaches, hydrophobic and antimicrobial coatings have emerged as promising preventive conservation solutions due to their ability to reduce water penetration, inhibit microbial growth, and limit biofilm formation on stone surfaces [2,12,24,27,28,34–37]. However, conventional protective coatings, including fluoropolymers, acrylics, siloxanes, and nanoparticle-based systems, often present important limitations such as low long-term durability, significant environmental toxicity, poor compatibility with porous substrates, reduced vapour permeability, and inducing visible chromatic alterations [4,16,24,26,30,33,35,38–44].

In recent years, increasing attention has been directed toward the development of sustainable and multifunctional coatings capable of combining hydrophobicity, antimicrobial activity, substrate compatibility, and environmental safety [4,12,19,27,34,45–49]. In this context, dendritic polymers have emerged as highly versatile macromolecular systems due to their well-defined branched architecture, high density of functional groups, tuneable surface chemistry, and multifunctional behaviour [2,4,30,34,45,47,49–56]. Dendrons, which differ from dendrimers, are dendritic macromolecular fragments with well-defined, controlled branching structures that exhibit particularly attractive properties for coating applications, including low viscosity, high reactivity, nanometric dimensions, and the possibility of incorporating amphiphilic functionalities [2,4,27,30,34,45–50,52–58].

In this study, new L-lysine-based dendritic coatings functionalized with fatty acids of different aliphatic chain lengths were developed for the protection of natural stone substrates. Among the different dendritic systems, L-lysine-based dendrons are considered to be especially promising due to the presence of multiple reactive amino groups that facilitate controlled branching and functionalization [47,48,51,57]. The incorporation of fatty acid chains into the dendritic architectures should provide hydrophobic behaviour while preserving compatibility with porous stone substrates [7,37,47,48,56].

The newly synthesized coatings were evaluated regarding their antimicrobial activity against biodeterioration-associated microorganisms, hydrophobic efficiency, vapour, colorimetric compatibility, and durability under accelerated weathering conditions. The obtained results intend to contribute to the development of innovative and sustainable multifunctional coatings for preventive conservation of stone cultural heritage.

2. Materials and Methods

2.1. Materials

2.1.1. Laboratory Consumables

L-lysine methyl ester dihydrochloride (Lys-COOMe·2HCl; ≥99%; CAS No. 26348-70-9), tetrahydrofuran (THF; ≥99.9%; CAS No. 109-99-9), *N*,*N*-dimethylformamide (DMF; ≥99.8%; CAS No. 68-12-2), methanol (≥99.8%; CAS No. 67-56-1), chloroform ($CHCl_3$; ≥99.8%; CAS No. 67-66-3), diethyl ether (Et_2O; ≥99.8%; CAS No. 60-29-7), sodium hydroxide (NaOH; ≥97.0%; CAS No. 1310-73-2), triethylamine (TEA; ≥99.5%; CAS No. 121-44-8), and HBTU (≥98.0%; CAS No. 94790-37-1) were purchased from Sigma-Aldrich (St. Louis, MO, USA) and used as received. Fatty acids with different aliphatic chain lengths were used for dendron functionalization, namely octanoic acid (C8:0; ≥99%; CAS No. 124-07-2), palmitic acid (C16:0; ≥99%; CAS No. 57-10-3), arachidic acid (C20:0; ≥99%; CAS No. 506-30-9), and behenic acid (C22:0; 99%; CAS No. 112-85-6) were purchased from TCI Chemicals (Tokyo, Japan) and used as received.

2.1.2. Stone Specimens

Three types of natural stone from quarries located in Portugal, commonly used in monuments, were selected: limestone, marble, and granite. The limestone was extracted from the Estremadura Limestone Massif and supplied by SOLANCIS—Sociedade Exploradora de Pedreiras, S.A. (Benedita, Portugal).; the marble originated from Vila Viçosa and was supplied by DIMPOMAR—Rochas Portuguesas, Lda. (Vila Viçosa, Portugal); and the granite was extracted from Alpalhão and supplied by FILSTONE—Comércio de Rochas, S.A. (Fátima, Portugal). These lithotypes were selected due to their frequent use in national built heritage and their distinct physical properties [12], allowing the performance of the coatings to be evaluated on substrates with different characteristics and enabling a comparative assessment [12,59].

The lithotype specimens were wet-cut into standard blocks measuring 3 × 3 × 0.4 cm using a cutting saw (DISCOPLAN-TS, Struers, Ballerup, Denmark). The surfaces were then polished with a carborundum polishing cloth (SiC P320, 46 µm) to obtain uniform surfaces and remove cutting imperfections. After polishing, the specimens were washed with distilled water, dried in an oven at 40 °C for 24 h, and allowed to cool to room temperature.

2.2. Methods

2.2.1. Synthesis of L-Lysine-Based Dendritic Polymers

L-lysine-based dendritic polymers were synthesized through a convergent synthetic methodology involving sequential amidation and hydrolysis reactions, adapted from previously reported procedures described by Agudo-Álvarez et al. [60] and Theodorou et al. [61]. Generation 0 dendrons (G0) were obtained through a two-step sequence involving HBTU-mediated coupling between L-lysine methyl ester dihydrochloride and the corresponding fatty acid to afford the methyl ester intermediates G0(COOMe)-R, followed by alkaline hydrolysis to yield the carboxylic acid derivatives G0(COOH)-R. The same synthetic sequence was subsequently applied using G0(COOH)-R as a precursor to obtain Generation 1 dendrons, G1(COOMe)-R and, after hydrolysis, the corresponding G1(COOH)-R dendrons. In the dendron nomenclature, R corresponds to the alkyl chains derived from octanoic,

palmitic, arachidic, and behenic acids, namely C7, C15, C19, and C21, respectively, after amide bond formation. The general synthetic pathway is shown in Figure 1.

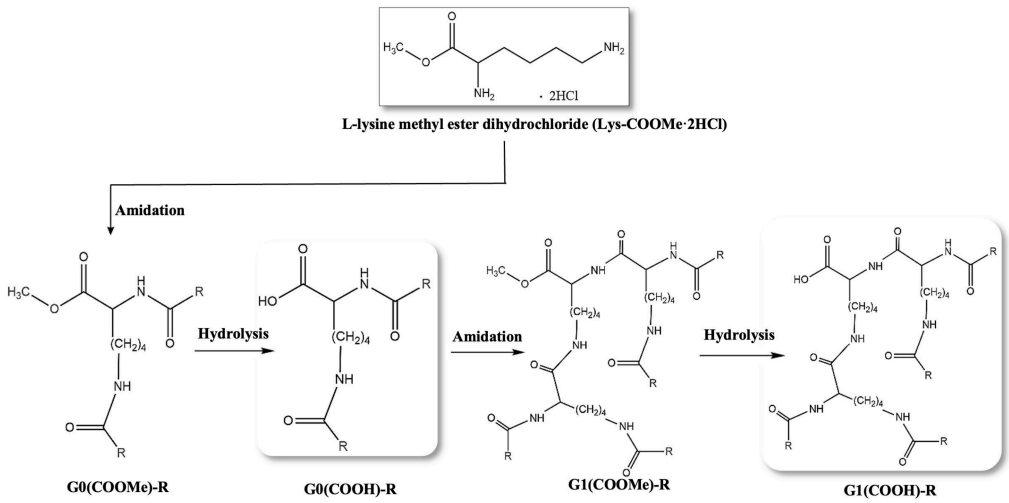


Figure 1. Reaction scheme involving L-lysine methyl ester dihydrochloride as starting material.

2.2.2. Structural Characterization of the Synthesized Compounds

The synthesized compounds were characterized by nuclear magnetic resonance (NMR), Fourier-transform infrared spectroscopy with attenuated total reflectance (FTIR-ATR), and electrospray ionization mass spectrometry (ESI-MS). ^{1}H and ^{13}C NMR spectra were recorded at 400 and 100 MHz, respectively, on an Avance III spectrometer (Bruker, Billerica, MA, USA), using $CDCl_3$ as solvent. Chemical shifts (δ) are reported in ppm. FTIR-ATR spectra were acquired on an Alpha Platinum-ATR spectrometer (Bruker, Billerica, MA, USA), in the 3500–500 cm^{-1} region. ESI-MS spectra were obtained using a Vanquish HPLC instrument (Thermo Fisher Scientific, Waltham, MA, USA) coupled to a DAD detector and an Orbitrap QExactive Focus mass spectrometer (Thermo Fisher Scientific, Waltham, MA, USA). The mass spectrometry analyses were performed at the Elemental Analysis, Chromatography and Mass Service of the University of Salamanca, Spain, while the remaining analyses were conducted at the University of Évora. The corresponding spectra and characterization data are provided in the Supplementary Information.

2.2.3. Preparation and Application of Coating Formulations

For the preparation of the dendritic polymer formulations, 50 mg of each synthesized compound were dispersed in 10 mL of a mixture of isopropanol/water (7:3, *v*/*v*). The resulting suspensions were homogenized by vortex agitation followed by ultrasonic treatment in order to obtain uniform formulations before application. The coatings were applied onto the stone surfaces by spray deposition, following the procedure described by Hashim et al. [12]: a spray gun connected to a Michelin MB24 air compressor (Bologna, Italy) operating at 230 V, with an air flow rate of 170 L/min and a maximum pressure of 8 bar, was used for the application. Each formulation was sprayed for approximately 3 s at a working distance of approximately 1 m from the stone surface to ensure homogeneous coverage. Because the coatings were applied by spray deposition onto porous stone substrates, a uniform and continuous film thickness could not be assumed. The coating thickness was, therefore, not determined, as the applied material may remain at the surface and/or partially penetrate the pore network depending on the formulation and substrate characteristics. Instead, the application procedure was standardised using the formulation concentration, application time, spraying distance, and operating conditions described

above. After application, all coated stone specimens were dried at room temperature for 24 h before subsequent assays.

2.2.4. Antimicrobial Activity Assays

The synthesized coatings were studied with the aim of evaluating their biocidal potential against microorganisms commonly found on stone substrates. For this purpose, two bacterial strains, *Bacillus cereus* and *Micrococcus* sp., and one yeast strain, *Saccharomyces cerevisiae*, were selected as representative microorganisms for the biological assays. Nutrient Agar (NA, HiMedia®) and Nutrient Broth (NB, Oxoid®) were used as solid and liquid culture media, respectively, for microbial growth throughout the experimental work. Culture media were prepared according to manufacturer recommendations and sterilized in an autoclave at 120 °C for 15 min prior to use in order to eliminate possible microbial contaminants. Stock solutions of the synthesized dendritic coatings were prepared at three different concentrations, namely 1000, 2000, and 5000 ppm, all in triplicate.

The antimicrobial activity assays were performed in sterile 96-well microplates, using an independent microplate for each microbial strain. For each well, 80 µL of NA or NB liquid culture medium and 10 µL of the corresponding dendritic coating solution were added for a final concentration of 100, 200 or 500 ppm of dendritic coating solution. Negative controls (blank assays) were prepared by replacing the coating solution with 10 µL of sterile Milli-Q water in order to evaluate microbial growth in the absence of coating influence. Microbial cells were resuspended in sterile Milli-Q water and 10 µL of the microbial suspension were added to each well, including blank controls. All antimicrobial activity procedures were carried out under aseptic conditions.

The microplates were incubated at 37 °C in a Multiskan GO UV–Vis spectrophotometer (Thermo Fisher Scientific, Waltham, MA, USA) with orbital shaking every 5 min until the control cultures (microorganism + sterile Milli-Q water) reached the stationary phase of microbial growth. Vancomycin hydrochloride (Sigma-Aldrich®) was used as positive control for *Micrococcus* sp. and *Bacillus cereus* assays, while Amphotericin B 80% (TCI®) was used as positive control for *Saccharomyces cerevisiae* assays.

2.2.5. Optical Tensiometry

Static water contact angle (θ) measurements were carried out using a Ramé-Hart Model 210 tensiometer (Succasunna, NJ, USA), following an experimental approach adapted from Armal et al. [2] and Hashim et al. [12]. Deionized water droplets of 12 µL were deposited onto the stone surface, and static contact angles were recorded between 3 and 10 s after droplet deposition using DROPimage software (ver. 3.21.11.0). For each specimen, five distinct droplets were deposited on the surface, and 15 measurements were recorded for each droplet. The final static contact angle value was expressed as the average of the measurements obtained for each surface. Measurements were performed before and after coating application, as well as after accelerated ageing, to evaluate the hydrophobic performance and durability of the treatments.

2.2.6. Colorimetric Analysis

Colorimetric measurements were performed according to the procedure described by Armal et al. [2], in order to evaluate whether the coatings preserved the original visual appearance of the stone surfaces after application and accelerated ageing. Measurements were carried out before and after coating application, and after accelerated ageing using a portable Konica Minolta colorimeter equipped with MAV aperture.

The colour parameters were expressed according to the CIELAB system, and the total colour difference (ΔE*) was calculated from the variations in L*, a*, and b* using Equation (1) [5,28,44,62,63].

$$\Delta E^* = \sqrt{\Delta L^{*2} + \Delta a^{*2} + \Delta b^{*2}} \quad (1)$$

According to the CIELAB colour system and heritage conservation criteria, colour differences become perceptible to the naked eye at ΔE values of approximately 1–2. In the conservation of built heritage, ΔE values below 5 are generally considered acceptable (ΔE* < 5) [2,64].

2.2.7. Accelerated Ageing Assays

The durability of the protective coatings was evaluated under simulated atmospheric conditions by accelerated weathering tests. Artificial ageing was performed in a QUV Accelerated Weathering Tester (Q-Lab Corporation, Westlake, OH, USA) following the ASTM G154 standard method [2,12]. The ageing protocol consisted of 15 min of water spray, followed by 3 h 45 min of condensation at 50 °C and 8 h of UVA irradiation at 340 nm and 60 °C, with an irradiance of 0.75 W/m^2, with a total of 28 cycles applied, each of which lasted 12 h, corresponding to a total testing period of 14 days.

After the artificial weathering tests, the durability of the coatings was assessed by repeating the static water contact angle measurements and colorimetric analyses. These tests allowed for the evaluation of the retention of the hydrophobic performance and the preservation of the aesthetic properties of the treated stone substrates after accelerated ageing.

3. Results and Discussion

3.1. Assessment of the Antimicrobial Potential

The antimicrobial potential of the synthesized dendritic coatings was evaluated against three microorganisms, namely *Bacillus cereus*, *Micrococcus* sp., and *Saccharomyces cerevisiae*.

3.1.1. Antimicrobial Potential Against *Bacillus cereus*

As illustrated in Table 1, among all synthesized formulations, only G1C7 exhibited significant antimicrobial activity against *Bacillus cereus*, with inhibition rates increasing from 11.0% at 100 ppm to 48.7% at 500 ppm. Vancomycin, used as the positive control, exhibited inhibition rates ranging from 27.7% to 38.0% against *Bacillus cereus*. Although vancomycin is an established antimicrobial agent against Gram-positive bacteria, including *Bacillus* species, the relatively limited inhibition observed under the present experimental conditions may be related to the specific susceptibility of the strain employed and/or the experimental conditions used. However, since the susceptibility of the tested strain to vancomycin was not independently characterized, no specific explanation can be established for the observed response. Interestingly, under the experimental conditions employed, G1C7 exhibited higher inhibition rates than vancomycin at 200 and 500 ppm (inhibition rates of 37.2% and 48.7%, respectively). This observation highlights the antimicrobial potential of G1C7 against the tested *B. cereus* strain, although direct comparison with vancomycin should be interpreted cautiously given the relatively limited inhibition observed for the reference antibiotic under the present assay conditions.

Table 1. Inhibition rate (expressed in %) of *Bacillus cereus* bacterial growth at three different concentrations of applied coatings, namely 100, 200, and 500 ppm.

Coating	100 ppm	200 ppm	500 ppm
G0C7	0	0	0
G1C7	11.0	37.2	48.7
G0C15	0	0	0
G1C15	0	0	0
G0C19	0	0	0
G1C19	0	0	0
G0C21	0	0	0
G1C21	0	0	0
Vancomycin	27.7	31.9	38.0

In contrast, the remaining formulations containing longer aliphatic chains (C15, C19, and C21) did not show detectable inhibitory activity against this bacterial strain. The progressive increase in inhibition observed for G1C7 with increasing concentration suggests a concentration-dependent antimicrobial effect associated with the interaction of the amphiphilic dendritic structure with the bacterial membrane. Amphiphilic compounds may disrupt bacterial membranes through destabilization of lipid bilayer organization, leading to loss of membrane integrity and subsequent inhibition of microbial growth [56,65–67].

The obtained results suggest the existence of an optimal hydrophobic–hydrophilic balance for membrane interaction, corresponding to the shorter aliphatic chain (C7). Longer hydrocarbon chains appear to increase the hydrophobic character of the dendritic structures, reducing their polarity and consequently limiting their dispersion and interaction with the bacterial membrane. Additionally, excessive hydrophobicity may hinder the accessibility of lysine-derived polar groups, which are responsible for electrostatic interactions with negatively charged phospholipids present in the bacterial membrane.

Interestingly, antimicrobial activity was only observed for the first-generation compound G1C7, whereas the corresponding generation 0 formulation (G0C7) did not exhibit inhibitory activity. This behaviour suggests that the higher density of lysine groups and hydrophobic tails present in the G1 dendritic structure enhances membrane interaction and destabilization. The increased density of positively charged lysine groups may favour electrostatic interactions with anionic membrane phospholipids, intensifying membrane disorganization and antimicrobial activity [56,65–67].

3.1.2. Antimicrobial Potential Against *Micrococcus* sp.

The G1C7 formulation also exhibited the highest antimicrobial performance against *Micrococcus* sp., with inhibition rates increasing from 22.5% at 200 ppm to 43.4% at 500 ppm (Table 2).

However, unlike *Bacillus cereus*, additional formulations containing longer aliphatic chains, namely G1C15, G1C19, and G1C21, also demonstrated inhibitory activity at lower concentrations, but this inhibition was not concentration-dependent. Fatty acid-containing amphiphilic compounds may promote membrane permeabilization through adsorption onto the microbial surface followed by insertion of hydrophobic segments into the lipid bilayer. This interaction destabilizes membrane organization and compromises cellular viability [56].

The observed differences between *Bacillus cereus* and *Micrococcus* sp. suggest distinct membrane susceptibilities associated with variations in membrane composition, lipid organization, and permeability. Similarly to the results obtained for *Bacillus cereus*, antimicrobial activity was predominantly observed for first-generation dendrons (G1), reinforcing the importance of higher lysine group density and amphiphilic organization in promoting

membrane interaction. Generation 0 compounds generally exhibited negligible activity, suggesting that the reduced number of lysine groups and hydrophobic tails limits effective interaction with the bacterial membrane.

Table 2. Inhibition rate (expressed in %) of *Micrococcus* sp. bacterial growth at three different concentrations of applied coatings, namely 100, 200, and 500 ppm.

Coating	100 ppm	200 ppm	500 ppm
G0C7	0	0	0
G1C7	0	22.5	43.4
G0C15	0	0	0
G1C15	10.6	0	0
G0C19	0	0	0
G1C19	2.4	0	0
G0C21	0.6	0	0
G1C21	15.1	0	0
Vancomycin	90.8	88.3	94.5

3.1.3. Antimicrobial Potential Against *Saccharomyces cerevisiae*

The antimicrobial assays performed against *Saccharomyces cerevisiae* revealed a broader inhibitory activity profile compared to the bacterial strains. All synthesized compounds exhibited some degree of antimicrobial activity against the yeast strain (Table 3), although substantial differences were observed depending on dendritic structure and concentration.

Table 3. Inhibition rate (expressed in %) of *Saccharomyces cerevisiae* bacterial growth at three different concentrations of applied coatings, namely 100, 200, and 500 ppm.

Coating	100 ppm	200 ppm	500 ppm
G0C7	0	0	46.0
G1C7	23.0	69.9	93.4
G0C15	40.0	0	0
G1C15	0	36.7	25.4
G0C19	22.9	0	0
G1C19	56.1	43.1	0
G0C21	52.6	29.5	0
G1C21	56.8	41.9	0
Amphotericin B	100.0	100.0	100.0

Among all formulations, G1C7 demonstrated the highest inhibitory activity, reaching 93.4% inhibition at 500 ppm. The strong concentration-dependent effect observed for this formulation is consistent with the results obtained for both bacterial strains, confirming the superior antimicrobial performance of the shorter-chain first-generation dendritic system. In contrast, several formulations containing longer aliphatic chains exhibited higher inhibition at lower concentrations, followed by reduced activity at higher concentrations. This behaviour was particularly evident for G1C15, G1C19, G0C21, and G1C21. Amphiphilic compounds may undergo concentration-dependent aggregation phenomena in aqueous media. The formation of molecular aggregates reduces the fraction of dispersed active molecules available to interact with microbial membranes, consequently decreasing antimicrobial efficiency [56,65–67]. The susceptibility of *Saccharomyces cerevisiae* to the synthesized coatings may also be associated with the structural complexity of the yeast membrane, which contains ergosterol as a major membrane component. Amphiphilic compounds may interact with sterol-containing membranes, inducing membrane destabilization and compromising essential cellular functions [56].

It should be noted that the antimicrobial assays performed in the present study used planktonic cells under controlled laboratory conditions. Although this approach provides a useful initial comparative assessment of the antimicrobial activity of the dendritic formulations, it does not reproduce the complexity of microbial biofilms developing on natural stone surfaces. Furthermore, the three microorganisms selected in this study, *Bacillus cereus*, *Micrococcus* sp. and *Saccharomyces cerevisiae*, represent only a limited fraction of the microbial diversity associated with stone biodeterioration. Therefore, the results should not be directly extrapolated to the efficacy of these formulations against established biofilms on heritage stone. Future studies should extend the range of microorganisms investigated and evaluate the antimicrobial performance of the coatings against biofilms developed on coated stone specimens under conditions representative of stone conservation applications.

3.2. Study of Hydrophobic Properties by Optical Tensiometry

The hydrophobic performance of the synthesized dendritic coatings was evaluated by optical tensiometry through static water contact angle (θ) measurements performed on marble, limestone, and granite substrates. These analyses aimed to assess both the initial hydrophobic efficacy of the coatings and the preservation of their water-repellent properties after accelerated ageing assays [2,12].

3.2.1. Study of the Effectiveness of Coatings

Hydrophobic coatings are generally considered effective when the treated surfaces exhibit static water contact angles higher than 90°. The results obtained for the different stone substrates are presented in Figure 2.

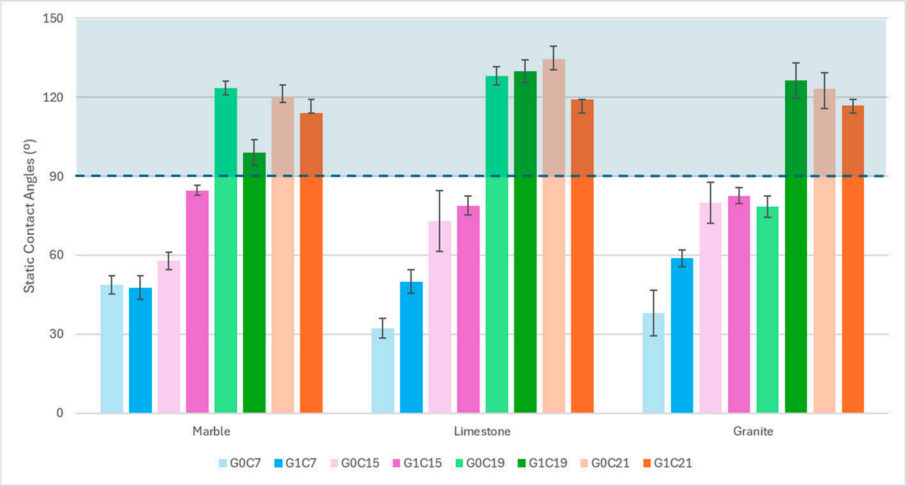


Figure 2. Graphical representation of the hydrophobic effectiveness of the applied coatings, based on the static contact angles of water measured in different lithotypes. The blue dashed line indicates the 90° threshold, corresponding to the lower limit used to classify a surface as hydrophobic, where the shaded blue area represents the hydrophobic coated surfaces.

The measured water contact angles varied according to both coating formulation and lithotype, confirming the influence of substrate characteristics and coating composition on surface wettability. Previous studies have linked substrate porosity to coating retention within the pore network [2,12]. However, as coating retention and penetration were not directly assessed in the present study, their contribution to the observed differences in water contact angles remains uncertain.

Hydrophobic behaviour ($\theta > 90°$) was mainly observed for formulations containing the longest fatty acid chains (C19 and C21), particularly on limestone and marble, whereas coatings incorporating shorter chains (C7 and C15) consistently exhibited contact angles below

90°. Overall, approximately 50% of the synthesized formulations displayed hydrophobic behaviour on at least one lithotype.

The higher contact angles observed for formulations containing C19 and C21 chains are consistent with the expected contribution of longer hydrocarbon chains to hydrophobic behaviour. However, surface free energy was not measured in this study, and contact angle measurements using water alone do not allow the polar and dispersive components of surface energy to be determined.

Differences in the measured contact angles may also be influenced by surface roughness and the distribution of the deposited material [12]. Nevertheless, coating morphology, thickness, and penetration into the stone pore network were not directly characterized. Consequently, the present results do not establish whether continuous surface films were formed or whether penetration into the substrate affected the amount of hydrophobic material exposed at the surface.

In any case, these results demonstrate that the hydrophobic performance of the synthesized dendritic coatings is strongly dependent on the length of the aliphatic fatty acid chains incorporated into the dendritic architecture.

3.2.2. Durability of Hydrophobic Coatings

The durability of the hydrophobic coatings was further evaluated through static contact angle measurements after accelerated ageing assays. The obtained post-ageing results are presented in Figure 3. The relative percentage variation between pre- and post-ageing contact angles is summarized in Table 4.

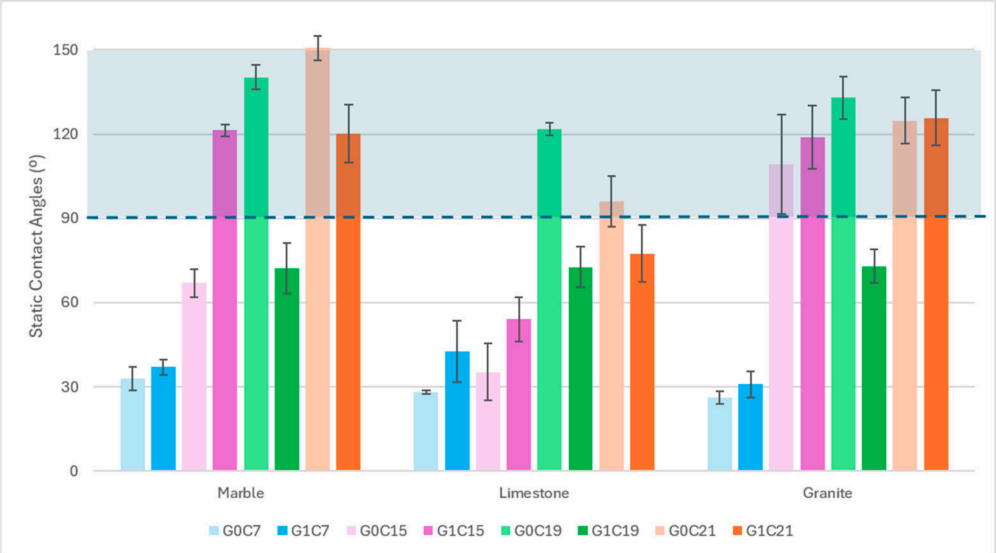


Figure 3. Graphical representation of the durability of the hydrophobic effectiveness of the applied coatings, based on the static contact angles of water measured on the different lithotypes after accelerated ageing testing. The blue dashed line indicates the 90° threshold, corresponding to the lower limit used to classify a surface as hydrophobic, where the shaded blue area represents the hydrophobic coated surfaces.

Accelerated weathering revealed that the durability of the hydrophobic coatings depended on both the lithotype and the coating formulation. Limestone exhibited the greatest loss of hydrophobic performance after ageing, whereas marble and granite generally showed higher coating stability. The lower durability observed for limestone is consistent with its higher porosity, which may facilitate water ingress and accelerate coating degradation [68].

Table 4. Relative percentage variation of static contact angles between pre- and post-ageing contact angles obtained before and after the accelerated ageing test for each coating applied to the different lithotypes under study.

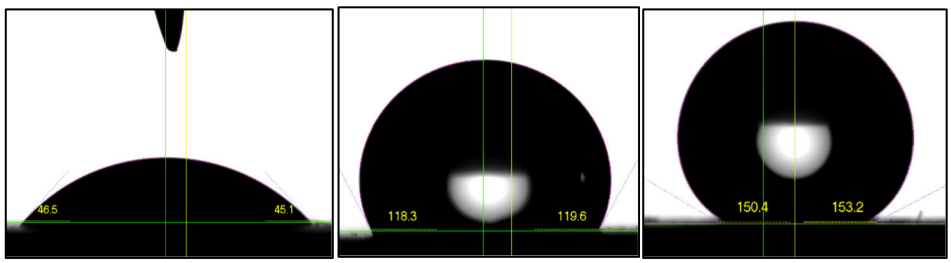
	Static Contact Angles (q)						Relative Percentage Variation in Contact Angles (%)		
	Pre-Ageing			Post-Ageing					
Coatings	**Marble**	**Limestone**	**Granite**	**Marble**	**Limestone**	**Granite**	**Marble**	**Limestone**	**Granite**
G0C7	48.7	32.2	38.0	32.9	28.2	26.3	−32.4	−12.4	−30.8
G1C7	47.6	50.0	58.7	37.0	42.5	30.9	−22.3	−15.0	−47.4
G0C15	57.9	73.0	79.9	67.0	35.3	109.3	15.7	−51.6	36.8
G1C15	84.6	78.8	82.6	121.3	54.1	118.9	43.4	−31.3	43.9
G0C19	123.6	128.2	78.4	140.2	121.8	132.9	13.4	−5.0	69.5
G1C19	99.0	129.9	126.5	72.2	72.6	73.0	−27.1	−44.1	−42.3
G0C21	120.1	134.4	123.3	150.6	96.0	124.8	25.4	−28.6	1.2
G1C21	113.9	119.2	116.8	120.2	77.5	125.8	5.5	−35.0	7.7

Among the synthesized formulations, G1C19 exhibited the most significant loss of hydrophobicity after ageing. Before weathering, this formulation presented contact angle values higher than 90° on all substrates, demonstrating effective hydrophobic behaviour. However, after accelerated ageing, all measured contact angles decreased below the hydrophobic threshold, corresponding to reductions of approximately 27%, 44%, and 42% for marble, limestone, and granite, respectively (Table 4). These results indicate substantial degradation of the hydrophobic surface properties under simulated environmental exposure.

Interestingly, several formulations exhibited improved hydrophobic behaviour after accelerated ageing, particularly on marble and granite substrates. G0C15, G0C19, and G1C15 showed substantial increases in contact angle values after weathering exposure. Notably, G1C15, which initially exhibited non-hydrophobic behaviour, achieved contact angles of approximately 121° on marble and 119° on granite after ageing (Table 4).

Similarly, G0C19 exhibited a remarkable 70% increase in contact angle values on granite after ageing, reaching approximately 133°, thereby acquiring effective hydrophobic behaviour that was not initially observed. Among all tested formulations, G0C21 demonstrated the highest hydrophobic durability. On marble substrates, this coating exhibited a 25% increase in contact angle after ageing, reaching values close to 151°, corresponding to superhydrophobic behaviour.

The optical tensiometry images presented in Figure 4 further illustrate the remarkable hydrophobicity achieved after ageing.



(**a**) (**b**) (**c**)

Figure 4. Optical tensiometry images obtained for the marble substrate: (**a**) contact angles of the uncoated stone (negative control); (**b**) contact angles after application of the G0C21 coating; (**c**) contact angles after ageing of the G0C21 coating.

Although some formulations exhibited higher water contact angles after accelerated ageing, the mechanisms underlying these changes cannot be determined from the present measurements alone. Changes in surface chemistry or organization, surface roughness, redistribution or partial removal of coating material, and changes in the polar and dispersive contributions to surface energy are possible explanations. However, these mechanisms remain hypotheses, as surface-energy components, coating morphology, thickness, penetration into the substrate, and adhesion were not independently assessed in this study. Further investigations incorporating complementary surface characterization techniques will be necessary to clarify the origin of the observed changes in wettability.

3.3. Evaluation of Chromatic Alteration in Lithotypes

The application of protective coatings onto natural stone substrates requires the preservation of the original aesthetic appearance of the treated materials. Among the different aesthetic parameters, colour variation is considered one of the most critical factors in cultural heritage conservation, since chromatic alterations are often macroscopically detected before any structural degradation becomes apparent [16]. Consequently, visible colour changes are generally considered undesirable in protective treatments for natural stone due to their potential impact on the historical, commercial and aesthetic value of the substrate.

3.3.1. Aesthetic Compatibility of the Synthesized Coatings

The chromatic compatibility of the synthesized dendritic coatings was evaluated using the CIELAB colour system. The obtained ΔE* values for the different lithotypes are presented in Figure 5.

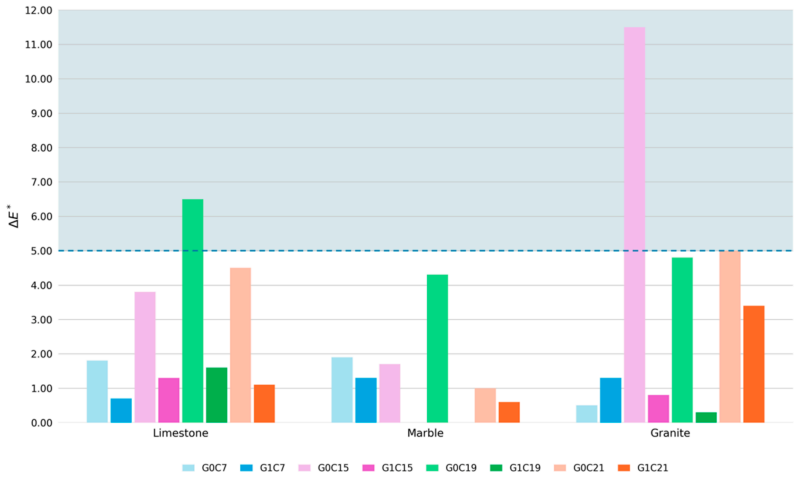


Figure 5. Graphical representation of ΔE* for coatings applied to limestone, marble, and granite stone samples. The shaded area represents the chromatic compatibility values considered to be unacceptable in the conservation of built heritage (ΔE* ≥ 5). Values below this threshold indicate limited colour differences, helping to preserve the original macroscopic appearance of the stone.

Most of the synthesized coatings exhibited satisfactory chromatic compatibility with the studied lithotypes, with ΔE values below the accepted conservation threshold (ΔE < 5). Marble showed excellent compatibility for all formulations, whereas limestone presented unacceptable colour variation only for G0C19, with the surface becoming visibly lighter and less glossy after coating application, suggesting partial surface accumulation and heterogeneous film formation, as demonstrated in Figure 6. Granite proved to be the most sensitive substrate, with G0C15 and G0C21 producing visible whitish surface alterations (Figure 6; ΔE* ≥ 5), indicating lower interfacial compatibility between these formulations and the substrate.

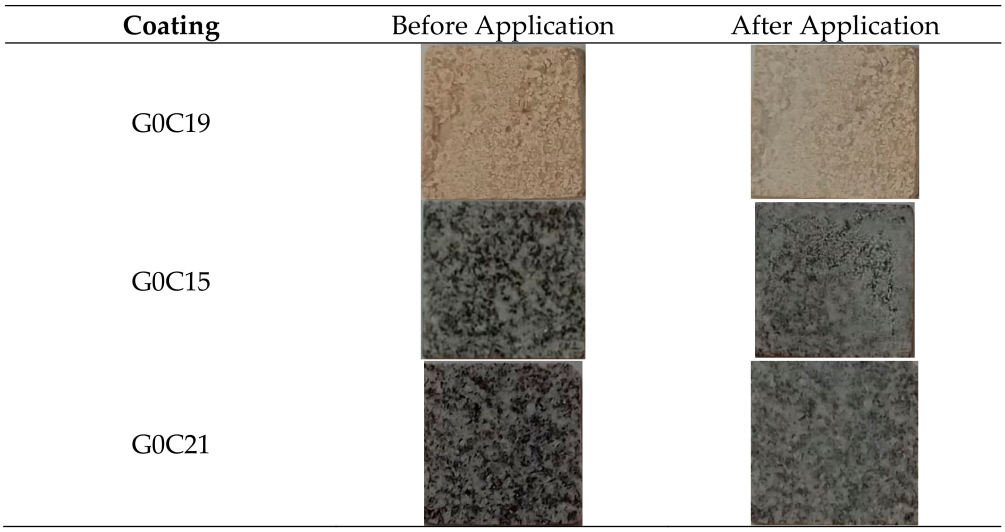


Figure 6. Photographic record of limestone and granite substrates before and after the application of G0C19, G0C15 and G0C21 coatings.

Overall, only 12.5% of the tested samples exceeded the acceptable colour variation limit, namely G0C19 on limestone and G0C15/G0C21 on granite, while all G1 formulations remained below this threshold. The improved performance of the G1 coatings characterized by a 1:4 ratio between carboxylic groups and hydrophobic chains may be attributed to their higher branching density and greater steric volume, which promote a more homogeneous interfacial organization and reduce heterogeneous surface accumulation. In contrast, the lower branching density of G0 systems, particularly those containing longer alkyl chains (C15–C21), may favour aggregation phenomena, resulting in localized chromatic alterations.

The lithotype properties may also influence coating behaviour. The greater porosity of limestone may facilitate coating penetration, reducing surface accumulation, whereas the low porosity and heterogeneous mineralogy of granite appear to promote less uniform coating distribution.

3.3.2. Effect of Accelerated Ageing on Chromatic Stability

In addition to initial chromatic compatibility, the long-term aesthetic stability of the coatings under environmental exposure is also a critical requirement for cultural heritage conservation applications. Therefore, after coating application, the stone substrates were subjected to accelerated ageing assays and subsequent colorimetric analyses were performed. The obtained ΔE^* values after artificial weathering are presented in Figure 7 and Table 5 summarizes the ΔE^* values obtained before and after the accelerated ageing test.

Overall, the coatings that initially exhibited satisfactory chromatic compatibility maintained this behaviour after accelerated ageing, confirming their long-term aesthetic stability under simulated environmental conditions. Interestingly, formulations previously considered chromatically incompatible, namely G0C19 on limestone and G0C21 on granite, exhibited substantial improvement after weathering exposure, reaching $\Delta E^* < 5$ after ageing (Table 5).

Photographic records presented in Figure 8 revealed partial recovery of the original stone coloration after ageing, particularly for G0C19 and G0C21, which became visibly less whitish after weathering exposure.

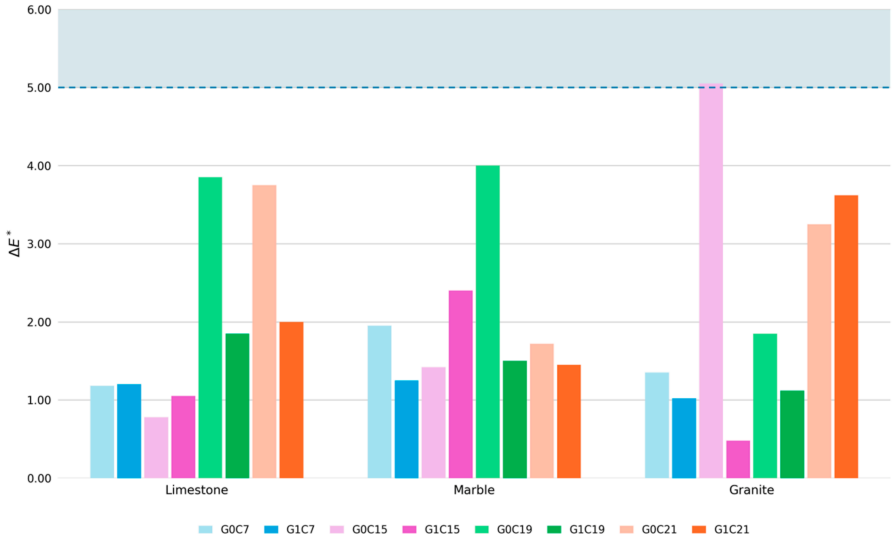


Figure 7. Graphical representation of ΔE* for the coatings applied to the stone samples under study after the ageing test. The shaded area represents the chromatic compatibility values considered to be unacceptable in the conservation of built heritage (ΔE* ≥ 5). Values below this threshold indicate limited colour differences, helping to preserve the original macroscopic appearance of the stone.

Table 5. ΔE* values obtained before and after the accelerated ageing test for each coating applied to the different lithotypes under study. Values shown in bold indicate ΔE* > 5.

	Colorimetric Analyses (ΔE*)					
	Pre-Ageing			**Post-Ageing**		
Coatings	**Marble**	**Limestone**	**Granite**	**Marble**	**Limestone**	**Granite**
G0C7	1.89	1.82	0.52	1.95	1.18	1.36
G1C7	1.27	0.72	1.25	1.26	1.21	1.04
G0C15	1.65	3.81	11.53	1.44	0.80	5.08
G1C15	1.09	1.31	0.78	2.42	1.07	0.49
G0C19	4.33	6.52	4.77	4.01	3.87	1.87
G1C19	0.31	1.60	0.31	1.52	1.89	1.14
G0C21	1.06	4.46	5.08	1.74	3.77	3.25
G1C21	0.59	1.13	3.41	1.47	2.01	3.64

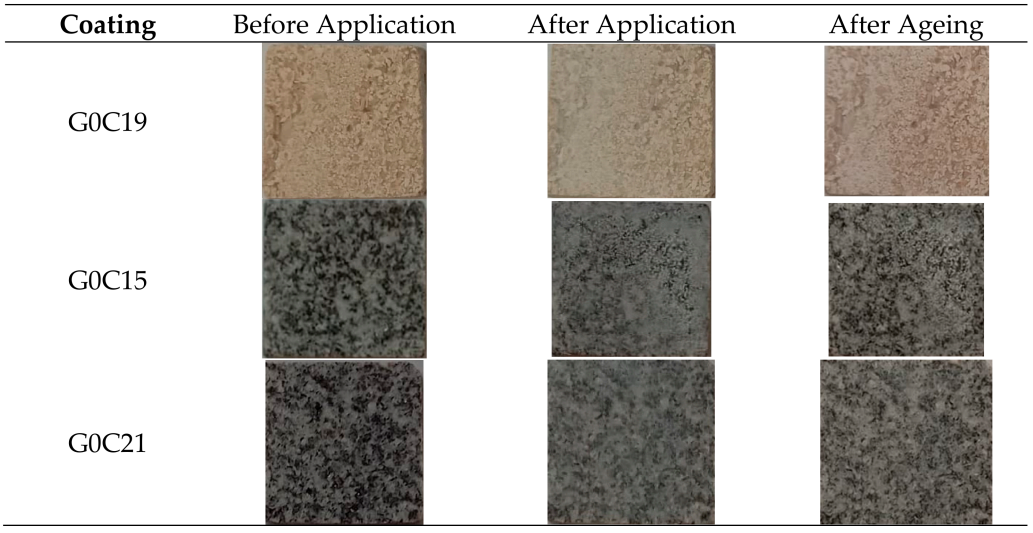


Figure 8. Photographic record of the limestone and granite substrates before and after the application of the G0C19, G0C15 and G0C21 coatings, as well as after the ageing test.

The partial recovery of the original coloration after accelerated ageing may be related to changes in the surface distribution of the coatings during exposure. These observations suggest that the response of the dendritic formulations to environmental ageing may depend on their interaction with the stone substrate, although further investigation would be needed to clarify the underlying processes.

4. Conclusions

In this study, a series of organic coatings based on L-lysine-derived dendrons functionalized with fatty acids of different aliphatic chain lengths were developed for the protection of natural stone substrates. The results obtained demonstrated that both dendritic generation and fatty acid chain length significantly influence the functional performance of the coatings. Overall, first-generation dendritic systems exhibited superior performance compared to their generation 0 counterparts.

Antimicrobial activity was found to be strongly influenced by dendritic architecture and fatty acid chain length. Shorter aliphatic chains, particularly in first-generation dendrons, promote enhanced antimicrobial performance due to a more favourable amphiphilic balance and improved interaction with microbial membranes. Conversely, excessive hydrophobicity associated with longer hydrocarbon chains may reduce molecular dispersion and promote aggregation phenomena, ultimately limiting antimicrobial efficiency.

The hydrophobicity of the synthesized dendritic coatings was also found to be strongly dependent on aliphatic chain length. The incorporation of longer aliphatic chains results in higher water static contact angles, suggesting that the increased hydrophobicity arises from the lower surface free energy associated with longer hydrocarbon chains. In turn, the durability of the hydrophobic coatings was found to be dependent on both substrate porosity and aliphatic chain length. Less porous substrates such as granite and marble favour long-term coating stability under the simulated environmental conditions tested, while longer hydrocarbon chains generally show greater resistance to environmental degradation. Several formulations displayed higher static water contact angles after accelerated ageing. However, the mechanisms underlying these changes remain unresolved, as surface-energy components, coating morphology, and coating–substrate adhesion were not directly measured. Chromatic compatibility was found to be dependent on both the molecular architecture of the dendritic coatings and the physicochemical characteristics of the stone substrate. Generation 1 formulations exhibited the highest chromatic compatibility, whereas some generation 0 coatings containing longer aliphatic chains induced visible colour alterations, likely due to aggregation phenomena and heterogeneous surface distribution. A large majority of the evaluated formulations (95.8%) exhibited acceptable chromatic compatibility after accelerated ageing, indicating that the newly synthesized dendritic coatings possess considerable potential for application in natural stone conservation, ensuring both long-term aesthetic preservation and functional durability under adverse environmental conditions.

The integrated assessment of the different performance parameters indicates that the developed coatings exhibit distinct functional profiles rather than a single formulation simultaneously maximising all evaluated properties. G1C7 showed the most relevant antimicrobial profile while maintaining good chromatic compatibility and ageing stability, whereas G0C21 provided a particularly favourable combination of hydrophobicity, aesthetic compatibility, and durability across the three lithotypes. These results highlight the importance of matching the coating formulation to the specific conservation requirements and physicochemical characteristics of the stone substrate.

Future studies may extend the assessment of these coatings by investigating additional properties relevant to stone conservation, including water vapour permeability, alongside

complementary characterisation of coating morphology, thickness, distribution, and adhesion. This broader approach will help clarify the interactions between the coatings and stone substrates and provide a more comprehensive understanding of their performance under conservation-relevant conditions.

Overall, the results obtained indicate that the developed dendritic coatings are promising multifunctional materials for natural stone conservation. Their organic nature makes them worth exploring as potential alternatives to conventional fluorinated protective treatments. However, their environmental performance and sustainability have not been assessed in the present study and would require further investigation, including dedicated evaluations of toxicity, biodegradability and environmental impact.

Supplementary Materials: The following supporting information can be downloaded at: https://www.mdpi.com/article/10.3390/app162110496/s1: Figure S1: 1H-NMR spectrum of the compound G0(COOH)-C15 obtained at $CDCl_3$, Figure S2: 13C-NMR spectrum of the compound G0(COOH)-C15 obtained at $CDCl_3$, Figure S3: FTIR spectrum of the compound G0(COOH)-C15, Figure S4: ESI-MS spectrum of the compound G0(COOH)-C15, Figure S5: 1H-NMR spectrum of the compound G1(COOH)-C15 obtained at $CDCl_3$, Figure S6: 13C-NMR spectrum of the compound G1(COOH)-C15 obtained at $CDCl_3$, Figure S7: FTIR spectrum of the compound G1(COOH)-C15, Figure S8: ESI-MS spectrum of the compound G1(COOH)-C15, Figure S9: 1H-NMR spectrum of the compound G0(COOH)-C7 obtained at $CDCl_3$, Figure S10: 13C-NMR spectrum of the compound G0(COOH)-C7 obtained at $CDCl_3$, Figure S11: FTIR spectrum of the compound G0(COOH)-C7, Figure S12: ESI-MS spectrum of the compound G0(COOH)-C7, Figure S13: 1H-NMR spectrum of the compound G1(COOH)-C7 obtained at $CDCl_3$, Figure S14: 13C-NMR spectrum of the compound G1(COOH)-C7 obtained at $CDCl_3$, Figure S15: FTIR spectrum of the compound G1(COOH)-C7, Figure S16: ESI-MS spectrum of the compound G1(COOH)-C7, Figure S17: 1H-NMR spectrum of the compound G0(COOH)-C19 obtained at $CDCl_3$, Figure S18: 13C-NMR spectrum of the compound G0(COOH)-C19 obtained at $CDCl_3$, Figure S19: FTIR spectrum of the compound G0(COOH)-C19, Figure S20: ESI-MS spectrum of the compound G0(COOH)-C19, Figure S21: 1H-NMR spectrum of the compound G1(COOH)-C19 obtained at $CDCl_3$, Figure S22: 13C-NMR spectrum of the compound G1(COOH)-C19 obtained at $CDCl_3$, Figure S23: FTIR spectrum of the compound G1(COOH)-C19, Figure S24: ESI-MS spectrum of the compound G1(COOH)-C19, Figure S25: 1H-NMR spectrum of the compound G0(COOH)-C21 obtained at $CDCl_3$, Figure S26: 13C-NMR spectrum of the compound G0(COOH)-C21 obtained at $CDCl_3$, Figure S27: FTIR spectrum of the compound G0(COOH)-C21, Figure S28: ESI-MS spectrum of the compound G0(COOH)-C21, Figure S29: 1H-NMR spectrum of the compound G1(COOH)-C21 obtained at $CDCl_3$, Figure S30: 13C-NMR spectrum of the compound G1(COOH)-C21 obtained at $CDCl_3$, Figure S31: FTIR spectrum of the compound G1(COOH)-C21 and Figure S32: ESI-MS spectrum of the compound G1(COOH)-C21.

Author Contributions: Conceptualization, P.B., S.M. and L.D.; methodology, P.B., S.M. and L.D.; validation, P.B., S.M., L.D., M.B., M.M.C. and M.C.; formal analysis, S.M., L.D., M.B., M.M.C. and M.C.; investigation, M.B. and M.M.C.; resources, P.B., A.T.C. and J.M.; data curation, M.B.; writing—original draft, M.B.; writing—review and editing, P.B., S.M., L.D., M.B., M.M.C., M.C., A.T.C. and J.M.; visualization, M.B.; supervision, P.B., S.M. and L.D.; project administration, P.B., S.M., L.D. and J.M.; funding acquisition, J.M. All authors have read and agreed to the published version of the manuscript.

Funding: This research was funded by the European Union's Recovery and Resilience Plan (NextGenerationEU), through the project "Sustainable Stone by Portugal—Valorization of natural stone for a digital, sustainable and qualified future", proposal no. C644943391-00000051, by the project "PROtection of built heritage through innovative TEChnologies" (ALT2030-FEDER-02680400), co-financed by the European Regional Development Fund (ERDF) through the Alentejo 2030 Regional Programme (ALENTEJO2030) and by the Foundation for Science and Technology, through pluriannual funding UID/04449/2025 (doi: 10.54499/UID/04449/2025), UID/PRR/04449/2025 (doi: 10.54499/UID/PRR/04449/2025) and LA/P/0132/2020 (doi: 10.54499/LA/P/0132/2020).

Institutional Review Board Statement: Not applicable.

Informed Consent Statement: Not applicable.

Data Availability Statement: Data is contained within the article or Supplementary Material.

Conflicts of Interest: The authors declare no conflicts of interest.

References

1. Alves, C.; Figueiredo, C.A.M.; Sanjurjo-Sánchez, J.; Hernández, A.C. Salt Weathering of Natural Stone: A Review of Comparative Laboratory Studies. *Heritage* **2021**, *4*, 1554–1565. [CrossRef]
2. Armal, F.; Dias, L.; Mirão, J.; Pires, V.; Sitzia, F.; Martins, S.; Costa, M.; Barrulas, P. Chemical Composition of Hydrophobic Coating Solutions and Its Impact on Carbonate Stones Protection and Preservation. *Sustainability* **2023**, *15*, 16135. [CrossRef]
3. Benavente, D.; de Jongh, M.; Cañaveras, J.C. Weathering Processes and Mechanisms Caused by Capillary Waters and Pigeon Droppings on Porous Limestones. *Minerals* **2021**, *11*, 18. [CrossRef]
4. Cao, Y.; Salvini, A.; Camaiti, M. Current Status and Future Prospects of Applying Bioinspired Superhydrophobic Materials for Conservation of Stone Artworks. *Coatings* **2020**, *10*, 353. [CrossRef]
5. Dias, L.; Rosado, T.; Candeias, A.; Mirão, J.; Caldeira, A.T. Linking Ornamental Stone Discolouration to Its Biocolonisation State. *Build. Environ.* **2020**, *180*, 106934. [CrossRef]
6. Dias, L.; Rosado, T.; Candeias, A.; Mirão, J.; Caldeira, A.T. A Change in Composition, a Change in Colour: The Case of Limestone Sculptures from the Portuguese National Museum of Ancient Art. *J. Cult. Herit.* **2020**, *42*, 255–262. [CrossRef]
7. Liu, P.; Chernyshov, A.; Najdi, T.; Fu, Y.; Dickerson, J.; Sandmeyer, S.; Jarboe, L. Membrane Stress Caused by Octanoic Acid in Saccharomyces Cerevisiae. *Appl. Microbiol. Biotechnol.* **2013**, *97*, 3239–3251. [CrossRef] [PubMed]
8. Siegesmund, S.; Weiss, T.; Vollbrecht, A. Natural Stone, Weathering Phenomena, Conservation Strategies and Case Studies: Introduction. *Geol. Soc. Lond. Spec. Publ.* **2002**, *205*, 1–7. [CrossRef]
9. Tiano, P. Biodeterioration of Stone Monuments a Worldwide Issue. *Open Conf. Proc. J.* **2016**, *7*, 29–38. [CrossRef]
10. Warscheid, T.; Braams, J. Biodeterioration of Stone: A Review. *Int. Biodeterior. Biodegrad.* **2000**, *46*, 343–368. [CrossRef]
11. Dias, L.; Pires, V.; Sitzia, F.; Lisci, C.; Candeias, A.; Caldeira, A.T.; Mirão, J. Evaluating the Biosusceptibility of Natural Stone as an Supporting Tool to Prevent Cultural Heritage Biodeterioration. *Eur. Phys. J. Plus* **2023**, *138*, 570. [CrossRef]
12. Hashim, H.; Dias, L.; Martins, S.; Pires, V.; Costa, M.; Barrulas, P. Optimization of the Application of Commercial Hydrophobic Coatings for Natural Stone Protection and Preservation. *Heritage* **2024**, *7*, 3495–3510. [CrossRef]
13. Liu, X.; Koestler, R.J.; Warscheid, T.; Katayama, Y.; Gu, J.D. Microbial Deterioration and Sustainable Conservation of Stone Monuments and Buildings. *Nat. Sustain.* **2020**, *3*, 991–1004. [CrossRef]
14. Sousa, L.M.O.; Suárez del Río, L.M.; Calleja, L.; Ruiz de Argandoña, V.G.; Rodríguez Rey, A. Influence of Microfractures and Porosity on the Physico-Mechanical Properties and Weathering of Ornamental Granites. *Eng. Geol.* **2005**, *77*, 153–168. [CrossRef]
15. Delgado Rodrigues, J. The Portuguese Lioz Stone: An Overview on the Deterioration Problems and Conservation Perspectives. *Geoheritage* **2022**, *14*, 23. [CrossRef]
16. Silva, I.; Dias, L.; Salvador, C.; Miller, A.Z.; Candeias, A.; Caldeira, A.T. Microbial Induced Stone Discoloration in Alcobaça Monastery: A Comprehensive Study. *J. Cult. Herit.* **2024**, *67*, 248–257. [CrossRef]
17. Scheerer, S.; Ortega-Morales, O.; Gaylarde, C. Microbial Deterioration of Stone Monuments—An Updated Overview. *Adv. Appl. Microbiol.* **2009**, *66*, 97–139. [CrossRef] [PubMed]
18. Rosado, T.; Dias, L.; Lança, M.; Nogueira, C.; Santos, R.; Martins, M.R.; Candeias, A.; Mirão, J.; Caldeira, A.T. Assessment of Microbiota Present on a Portuguese Historical Stone Convent Using High-Throughput Sequencing Approaches. *Microbiologyopen* **2020**, *9*, 1067–1084. [CrossRef] [PubMed]
19. Campostrini, A.; Sala-Luis, A.; Bosch-Roig, P.; Ghedini, E.; Signoretto, M.; Menegazzo, F. Mesoporous Silica and Vegetal Extracts Combined as Sustainable Stone Heritage Protection against Biodeterioration. *Appl. Microbiol. Biotechnol.* **2025**, *109*, 99. [CrossRef] [PubMed]
20. Sterflinger, K.; Piñar, G. Microbial Deterioration of Cultural Heritage and Works of Art—Tilting at Windmills? *Appl. Microbiol. Biotechnol.* **2013**, *97*, 9637–9646. [CrossRef] [PubMed]
21. Gaylarde, C.C.; Baptista-Neto, J.A. Microbiologically Induced Aesthetic and Structural Changes to Dimension Stone. *npj Mater. Degrad.* **2021**, *5*, 33. [CrossRef]
22. Silva, I.; Salvador, C.; Miller, A.Z.; Candeias, A.; Caldeira, A.T. The Role of Bacteria in Pink Stone Discoloration: Insights from Batalha Monastery. *Micro* **2024**, *4*, 778–797. [CrossRef]
23. Sterflinger, K. Fungi: Their Role in Deterioration of Cultural Heritage. *Fungal Biol. Rev.* **2010**, *24*, 47–55. [CrossRef]
24. Mu, B.; Ying, X.; Petropoulos, E.; He, S. Preparation of AgCl/ZnO Nano-Composite for Effective Antimicrobial Protection of Stone-Made Building Elements. *Mater. Lett.* **2021**, *285*, 129143. [CrossRef]

25. Lewis, F.J.; May, E.; Bravery, A.F. Metabolic Activities of Bacteria Isolated from Building Stone and Their Relationship to Stone Decay. In *Biodeterioration 7*; Houghton, D.R., Smith, R.N., Eggins, H.O.W., Eds.; Springer: Dordrecht, The Netherlands, 1988; pp. 107–112. [CrossRef]
26. Romani, M.; Warscheid, T.; Nicole, L.; Marcon, L.; Di Martino, P.; Suzuki, M.T.; Lebaron, P.; Lami, R. Current and Future Chemical Treatments to Fight Biodeterioration of Outdoor Building Materials and Associated Biofilms: Moving Away from Ecotoxic and towards Efficient, Sustainable Solutions. *Sci. Total Environ.* **2022**, *802*, 149846. [CrossRef] [PubMed]
27. Latthe, S.S.; Terashima, C.; Nakata, K.; Fujishima, A. Superhydrophobic Surfaces Developed by Mimicking Hierarchical Surface Morphology of Lotus Leaf. *Molecules* **2014**, *19*, 4256–4283. [CrossRef] [PubMed]
28. Eyssautier-Chuine, S.; Calandra, I.; Vaillant-Gaveau, N.; Fronteau, G.; Thomachot-Schneider, C.; Hubert, J.; Pleck, J.; Gommeaux, M. A New Preventive Coating for Building Stones Mixing a Water Repellent and an Eco-Friendly Biocide. *Prog. Org. Coat.* **2018**, *120*, 132–142. [CrossRef]
29. Stanaszek-Tomal, E. Environmental Factors Causing the Development of Microorganisms on the Surfaces of National Cultural Monuments Made of Mineral Building Materials—Review. *Coatings* **2020**, *10*, 1203. [CrossRef]
30. Collins, C.M.; Safiuddin, M. Lotus-Leaf-Inspired Biomimetic Coatings: Different Types, Key Properties, and Applications in Infrastructures. *Infrastructures* **2022**, *7*, 46. [CrossRef]
31. Noiriel, C.; Gouze, P.; Bernard, D. Investigation of Porosity and Permeability Effects from Microstructure Changes during Limestone Dissolution. *Geophys. Res. Lett.* **2004**, *31*, L24603. [CrossRef]
32. Ding, X.; Lan, W.; Gu, J.D. A Review on Sampling Techniques and Analytical Methods for Microbiota of Cultural Properties and Historical Architecture. *Appl. Sci.* **2020**, *10*, 8099. [CrossRef]
33. Cappitelli, F.; Cattò, C.; Villa, F. The Control of Cultural Heritage Microbial Deterioration. *Microorganisms* **2020**, *8*, 1542. [CrossRef] [PubMed]
34. Căta, A.; Ienașcu, I.M.C.; Ştefănuț, M.N.; Roșu, D.; Pop, O.R. Properties and Bioapplications of Amphiphilic Janus Dendrimers: A Review. *Pharmaceutics* **2023**, *15*, 589. [CrossRef] [PubMed]
35. Fermo, P.; Cappelletti, G.; Cozzi, N.; Padeletti, G.; Kaciulis, S.; Brucale, M.; Merlini, M. Hydrophobizing Coatings for Cultural Heritage. A Detailed Study of Resin/Stone Surface Interaction. *Appl. Phys. A Mater. Sci. Process.* **2014**, *116*, 341–348. [CrossRef]
36. Jafari, R.; Asadollahi, S.; Farzaneh, M. Applications of Plasma Technology in Development of Superhydrophobic Surfaces. *Plasma Chem. Plasma Process.* **2013**, *33*, 177–200. [CrossRef]
37. Yoon, B.K.; Jackman, J.A.; Valle-González, E.R.; Cho, N.-J. Antibacterial Free Fatty Acids and Monoglycerides: Biological Activities, Experimental Testing, and Therapeutic Applications. *Int. J. Mol. Sci.* **2018**, *19*, 1114. [CrossRef] [PubMed]
38. Ibrahim, M.M.; Mohamed, W.S.; Mohamed, H.M. Experimental Study for Evaluation of Paraloid® B72 and Its Nanocomposite with Nano TiO2 and Nano ZnO for Consolidation of Pottery Samples. *Sci. Cult.* **2021**, *7*, 101–111. [CrossRef]
39. Trovão, J.; Portugal, A. Evaluation of the Antifungal Efficiency of Biocides Currently Applied in the Coimbra UNESCO Area Limestone Monuments. *Conserv. Patrim.* **2023**, *42*, 7–16. [CrossRef]
40. Valenzuela, L.; Iglesias-Juez, A.; Bachiller-Baeza, B.; Faraldos, M.; Bahamonde, A.; Rosal, R. Biocide Mechanism of Highly Efficient and Stable Antimicrobial Surfaces Based on Zinc Oxide-Reduced Graphene Oxide Photocatalytic Coatings. *J. Mater. Chem. B* **2020**, *8*, 8294–8304. [CrossRef] [PubMed]
41. Takayanagi, T.; Yamabe, M. Progress of Fluoropolymers on Coating Applications: Development of Mineral Spirit Soluble Polymer and Aqueous Dispersion. *Prog. Org. Coat.* **2000**, *40*, 185–190. [CrossRef]
42. Vinçotte, A.; Beauvoit, E.; Boyard, N.; Guilminot, E. Effect of Solvent on PARALOID® B72 and B44 Acrylic Resins Used as Adhesives in Conservation. *Herit. Sci.* **2019**, *7*, 42. [CrossRef]
43. Fidanza, M.R.; Caneva, G. Natural Biocides for the Conservation of Stone Cultural Heritage: A Review. *J. Cult. Herit.* **2019**, *38*, 271–286. [CrossRef]
44. Gabriele, F.; Casieri, C.; Vetrano, A.; Spreti, N. Evaluation of Acrylic and Silane Coatings on Limestone through Macroscopic and Microscopic Analyses. *Mater. Chem. Phys.* **2023**, *307*, 128194. [CrossRef]
45. Meleán Brito, R.S.; Padró, J.M.; Villa-Pérez, C.; Strumia, M.C.; Mattea, F.; Milanesio, J.M. Hydrophobic Dendritic Modification of a Poly(Acrylamide-Co-Acrylic Acid) Copolymer with Behera's Amine as Viscous Agent. *Ind. Eng. Chem. Res.* **2024**, *63*, 13580–13589. [CrossRef]
46. Karapanagiotis, I.; Manoudis, P.N. Superhydrophobic and Superamphiphobic Materials for the Conservation of Natural Stone: An Overview. *Constr. Build. Mater.* **2022**, *320*, 126175. [CrossRef]
47. Lyu, Z.; Ding, L.; Huang, A.Y.T.; Kao, C.L.; Peng, L. Poly(Amidoamine)Dendrimers: Covalent and Supramolecular Synthesis. *Mater. Today Chem.* **2019**, *13*, 34–48. [CrossRef]
48. Sowinska, M.; Urbanczyk-Lipkowska, Z. Advances in the Chemistry of Dendrimers. *New J. Chem.* **2014**, *38*, 2168–2203. [CrossRef]
49. Walter, M.V.; Malkoch, M. Simplifying the Synthesis of Dendrimers: Accelerated Approaches. *Chem. Soc. Rev.* **2012**, *41*, 4593–4609. [CrossRef] [PubMed]

50. Ledin, P.A.; Friscourt, F.; Guo, J.; Boons, G.J. Convergent Assembly and Surface Modification of Multifunctional Dendrimers by Three Consecutive Click Reactions. *Chem. Eur. J.* **2011**, *17*, 839–846. [CrossRef] [PubMed]
51. Tomalia, D.A.; Christensen, J.B.; Boas, U. *Dendrimers, Dendrons, and Dendritic Polymers: Discovery, Applications, and the Future*; Cambridge University Press: Cambridge, UK, 2012. [CrossRef]
52. Tully, D.C.; Fréchet, J.M.J. Dendrimers at Surfaces and Interfaces: Chemistry and Applications. *Chem. Commun.* **2001**, *2*, 1229–1239. [CrossRef]
53. Ya-Ting Huang, A.; Kao, C.L.; Selvaraj, A.; Peng, L. Solid-Phase Dendrimer Synthesis: A Promising Approach to Transform Dendrimer Construction. *Mater. Today Chem.* **2023**, *27*, 101285. [CrossRef]
54. Abbasi, E.; Aval, S.F.; Akbarzadeh, A.; Milani, M.; Nasrabadi, H.T.; Joo, S.W.; Hanifehpour, Y.; Nejati-Koshki, K.; Pashaei-Asl, R. Dendrimers: Synthesis, Applications, and Properties. *Nanoscale Res. Lett.* **2014**, *9*, 247. [CrossRef] [PubMed]
55. Adronov, A.; Frechet, J.M.J. Light-Harvesting Dendrimers. *Chem. Commun.* **2000**, *36*, 1701–1710. [CrossRef]
56. Desbois, A.P.; Smith, V.J. Antibacterial Free Fatty Acids: Activities, Mechanisms of Action and Biotechnological Potential. *Appl. Microbiol. Biotechnol.* **2010**, *85*, 1629–1642. [CrossRef] [PubMed]
57. Chabre, Y.M.; Roy, R. Design and Creativity in Synthesis of Multivalent Neoglycoconjugates. *Adv. Carbohydr. Chem. Biochem.* **2010**, *63*, 165–393. [CrossRef] [PubMed]
58. Li, J.; Sha, Y. A Convenient Synthesis of Amino Acid Methyl Esters. *Molecules* **2008**, *13*, 1111–1119. [CrossRef] [PubMed]
59. Dias, L.; Nunes, R.; Costa, M.; Caldeira, A.T.; Mirão, J.; Barrulas, P. Unveiling the Effectiveness of Innovative Commercial Coatings Used for the Preservation of Natural Stone—A Contribution. *Heritage* **2023**, *6*, 6328–6342. [CrossRef]
60. Agudo-Álvarez, S.; Díaz-Mínguez, S.S.; Benito-Arenas, R. The Amide Group and Its Preparation Methods by Acid-Amine Coupling Reactions: An Overview. *Pure Appl. Chem.* **2024**, *96*, 691–707. [CrossRef]
61. Theodorou, V.; Skobridis, K.; Tzakos, A.G.; Ragoussis, V. A Simple Method for the Alkaline Hydrolysis of Esters. *Tetrahedron Lett.* **2007**, *48*, 8230–8233. [CrossRef]
62. Silva, I.; Salvador, C.; Miller, A.Z.; Candeias, A.; Caldeira, A.T. Addressing Biodeterioration at UNESCO Stone Monuments: Tomar Convent and Batalha Monastery. *Int. Biodeterior. Biodegrad.* **2025**, *205*, 106188. [CrossRef]
63. Prieto, B.; Sanmartín, P.; Silva, B.; Martínez-Verdú, F. Measuring the Color of Granite Rocks: A Proposed Procedure. *Color Res. Appl.* **2010**, *35*, 368–375. [CrossRef]
64. Munafò, P.; Goffredo, G.B.; Quagliarini, E. TiO_2-Based Nanocoatings for Preserving Architectural Stone Surfaces: An Overview. *Constr. Build. Mater.* **2015**, *84*, 201–218. [CrossRef]
65. Sut, T.N.; Yoon, B.K.; Jackman, J.A. Synergistic Membrane Disruption of E. coli Tethered Lipid Bilayers by Antimicrobial Lipid Mixtures. *Biomimetics* **2025**, *10*, 739. [CrossRef] [PubMed]
66. Zhang, N.; Dhumal, D.; Kuo, S.H.; Lew, S.Q.; Patil, P.D.; Taher, R.; Vaidya, S.; Galanakou, C.; Elkihel, A.; Oh, M.W.; et al. Targeting the Phosphatidylglycerol Lipid: An Amphiphilic Dendrimer as a Promising Antibacterial Candidate. *Sci. Adv.* **2024**, *10*, eadn8117. [CrossRef] [PubMed]
67. Jennings, J.; Ašćerić, D.; Semeraro, E.F.; Lohner, K.; Malanovic, N.; Pabst, G. Combinatorial Screening of Cationic Lipidoids Reveals How Molecular Conformation Affects Membrane-Targeting Antimicrobial Activity. *ACS Appl. Mater. Interfaces* **2023**, *15*, 40178–40190. [CrossRef] [PubMed]
68. Ortiz-Marqués, A.; Caldevilla, P.; Goldmann, E.; Safuta, M.; Fernández-Raga, M.; Górski, M. Porosity and Permeability in Construction Materials as Key Parameters for Their Durability and Performance: A Review. *Buildings* **2025**, *15*, 3422. [CrossRef]

Disclaimer/Publisher's Note: The statements, opinions and data contained in all publications are solely those of the individual author(s) and contributor(s) and not of MDPI and/or the editor(s). MDPI and/or the editor(s) disclaim responsibility for any injury to people or property resulting from any ideas, methods, instructions or products referred to in the content.